Supplement of

Amplification of light absorption of black carbon associated with air pollution

Yuxuan Zhang[1,2], Qiang Zhang[1], Yafang Cheng[3,2], Hang Su[3,2], Haiyan Li[4], Meng Li[1,2], Xin Zhang[1], Aijun Ding[5], and Kebin He[4]

[1]Ministry of Education Key Laboratory for Earth System Modeling, Department of Earth System Science, Tsinghua University, Beijing 100084, China

[2]Multiphase Chemistry Department, Max Planck Institute for Chemistry, Mainz 55020, Germany

[3]Institute for Environmental and Climate Research, Jinan University, Guangzhou 510630, China

[4]State Key Joint Laboratory of Environment Simulation and Pollution Control, School of Environment, Tsinghua University, Beijing 100084, China

[5]Institute for Climate and Global Change Research, School of Atmospheric Sciences, Nanjing University, Nanjing, China

Correspondence to: Qiang Zhang (qiangzhang@tsinghua.edu.cn)

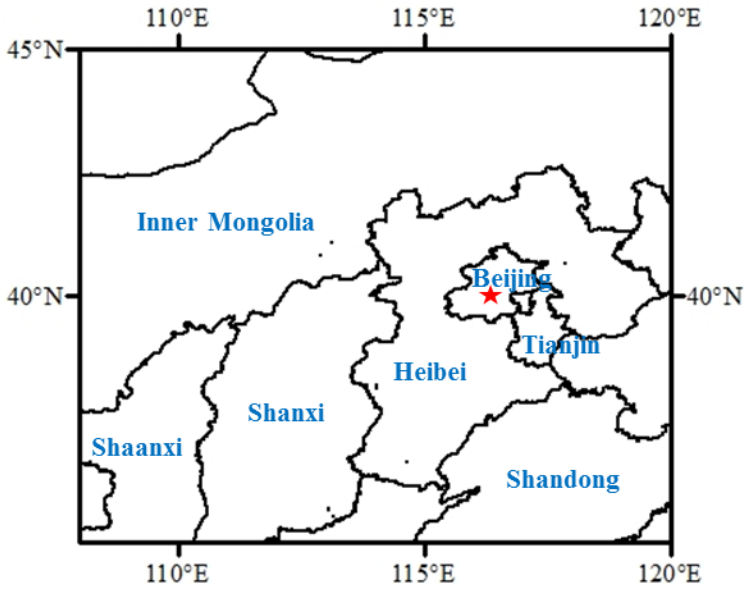

Figure S1. Location of the observation site (red star).

Figure S1 shows the geographic location of our observation site (namely red star marked in the Fig. S4). The site (40º00'17" N, 116º19'34" E) is located in megacity Beijing, the capital of China. The air pollution levels in our site can be influence by the air mass from adjacent regions (i.e., Tianjin, Heibei, Inner Mongolia, Shanxi, Shandong).

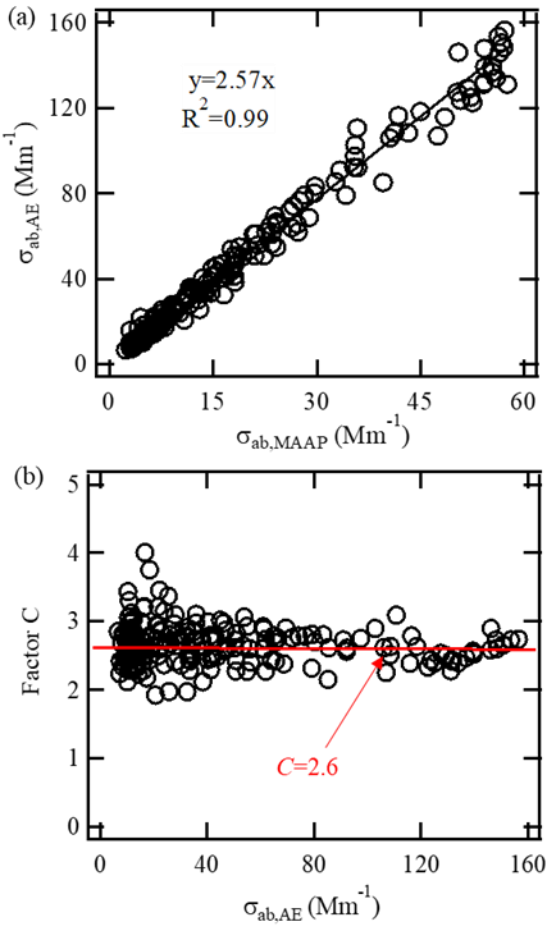

Figure S2. (a) The correlation between the absorption coefficient from AE33 at 660 nm ($\sigma_{ab,AE}$) and MAAP at 670 nm ($\sigma_{ab,MAAP}$). (b) Variety of multiple-scattering compensation factor *C* with different Aethalometer measurements.

Aethalometer artefacts are mainly from the loading effect and multiple-scattering effect (Weingartner et al., 2003; Segura et al., 2014). In terms of the loading effect, the compensation algorithm has been incorporated into Aethalometer model AE33 (Drinovec et al., 2015). In this study, we focused on the multiple-scattering compensation, which was characterized by enhancement parameter *C*. The factor *C* for our sites was determined by comparing the absorption coefficient derived from AE33 ($\sigma_{ab,AE}$) with the ones from MAAP ($\sigma_{ab,MAAP}$). As shown in Fig. S2a, the slope 2.6 was taken as the value of factor *C* to compensate the Aethalometer data. The specifically site-calculated values of the factor *C* varies in the range of 1.9-4 in this work (Fig. S2b), consistent with previous studies (Drinovec et al., 2015; Weingartner et al., 2003; Segura et al., 2014). Considering using a constant of 2.6 to simplify

calculation, the uncertainty of the factor C is about ~10%, which would lead to an uncertainty of ~10% in absorption coefficient derived from Aethalometer measurements.

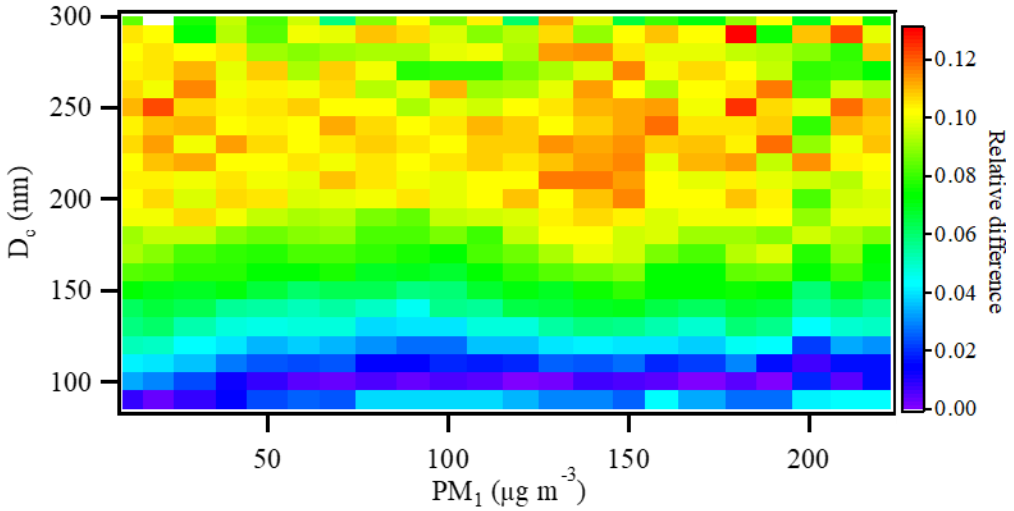

Figure S3. The relative difference between the sizes of BC-containing particles (D_p) derived from Mie calculation with RI_c of 2.26-1.26i and 1.95-0.79i.

Various values (e.g., 2.26-1.26i, 1.95-0.79i) of refractive index of BC core (RI_c) have be used in literature (Bond and Bergstrom, 2006; Cappa et al., 2012; Taylor et al., 2015). Figure S3 shows the relative difference between the sizes of BC-containing particles (D_p) derived from Mie calculation with RI_c of 2.26-1.26i and 1.95-0.79i. For BC-containing particles with 75-300 nm rBC cores, the relative difference is 3-10%, indicating that the D_p values were not sensitive to RI_c values in our study. This could be attributed to larges of coating materials on BC surface in our site.

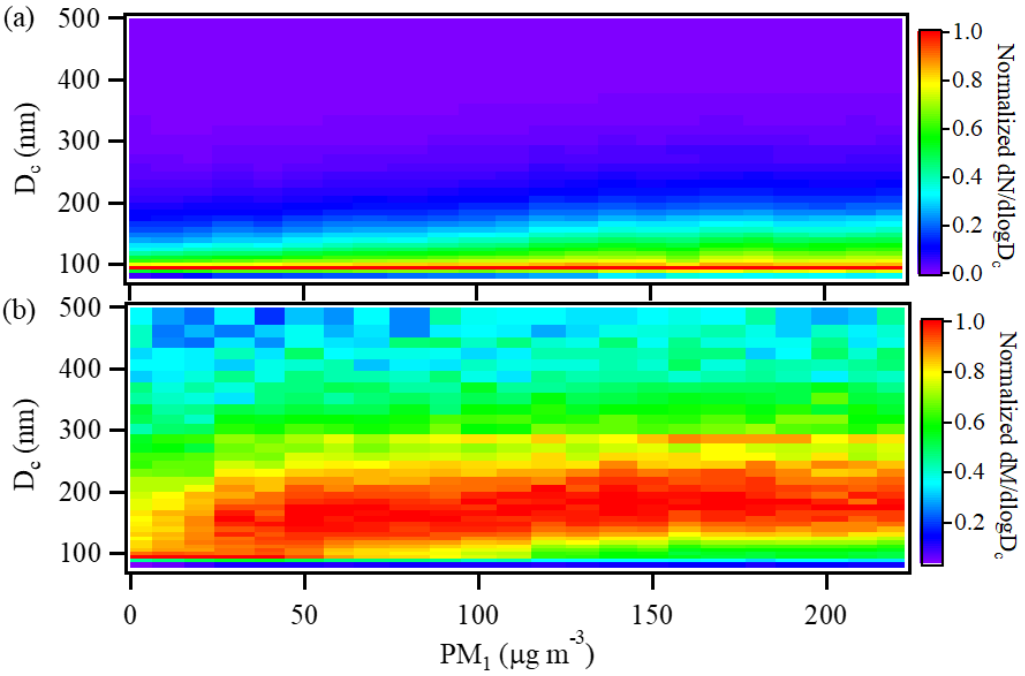

Figure S4. Size distribution of refractory BC (rBC) as a function of the PM_1 concentration: (a) number size distribution and (b) mass size distribution.

Figure S4 shows the size distribution of rBC as a function of the PM_1 concentration. Above the detection limit of SP2 incandescence (rBC with size larger than ~75 nm), the number size distribution of rBC cores shows a peak at ~95 nm under different PM_1 concentration (Fig. S4 (a)), and there are about 95% of rBC particles in number concentration lower than 200 nm. As shown in Fig. S4 (b)), the mass size distribution of rBC cores shows a wide mode at ~95-200 nm under different PM concentration.

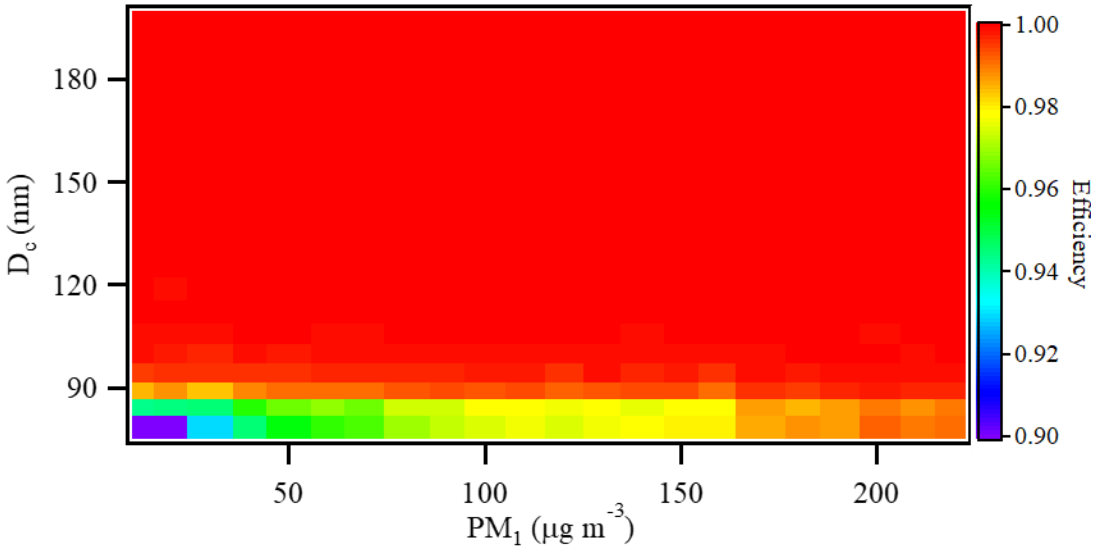

Figure S5. The detect efficiency of SP2 scattering for BC-containing particles with size-resolved rBC cores (75-200 nm) under different PM_1 concentration. In this study, the detect efficiency of SP2 scattering in terms of BC-containing particles at a certain rBC core size is defined as the ratio of the number concentration of particles above the detection limit of SP2 scattering and total particles.

Figure S5 shows the detect efficiency of SP2 scattering for BC-containing particles with size-resolved rBC cores (75-200 nm) under different PM_1 concentration. For BC-containing particles above the detection limit of our SP2 incandescence (rBC cores larger than ~75 nm), the detect efficiency of SP2 scattering is defined as the ratio of the number concentration of particles above the detection limit of SP2 scattering and total particles. The SP2 scattering exhibited a high detection efficiency (90-100%) for observed BC-containing particles with rBC cores more than 75 nm, which could be attributed to large BC-containing particles (~180-500 nm shown in Fig. S6) in our site due to atmospheric aging. High detection efficiency of SP2 scattering is favor to retrieve the thickness of coating materials on rBC cores (>75 nm size studied in this work) based on scattering signal.

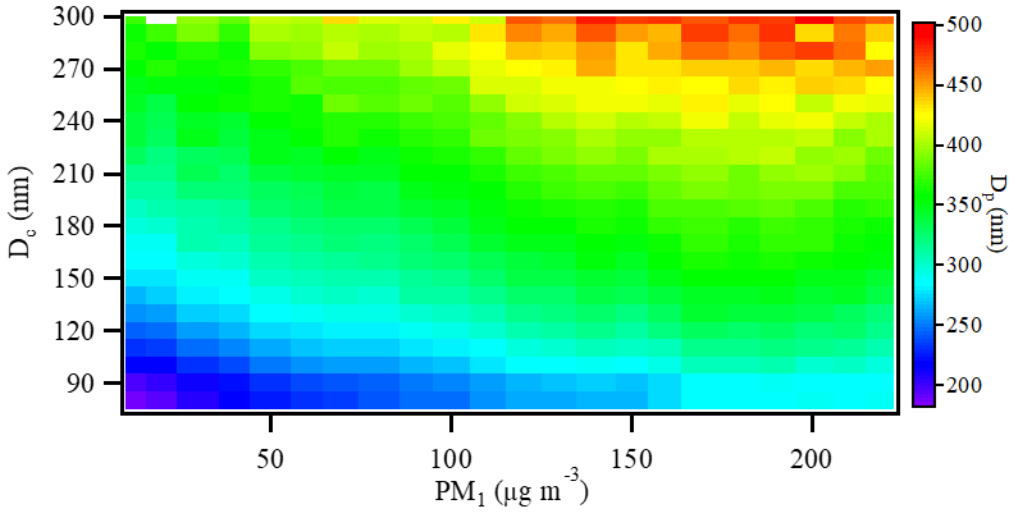

Figure S6. Frequency of the D_p/D_c ratio of BC-containing particles with size-resolved rBC cores as a function of PM1 concentrations.

Figure S6 shows frequency distribution of the D_p/D_c ratio of BC-containing particles with size-resolved rBC cores under different PM_1 concentrations. For BC-containing particles with 75-300 nm rBC cores, their particle size was in the range of 180-500 nm. The particle size (D_p) of BC-containing particles with rBC cores at a certain size significantly increased with increasing PM_1 concentration, revealing more coating materials on BC surface under more polluted environment.

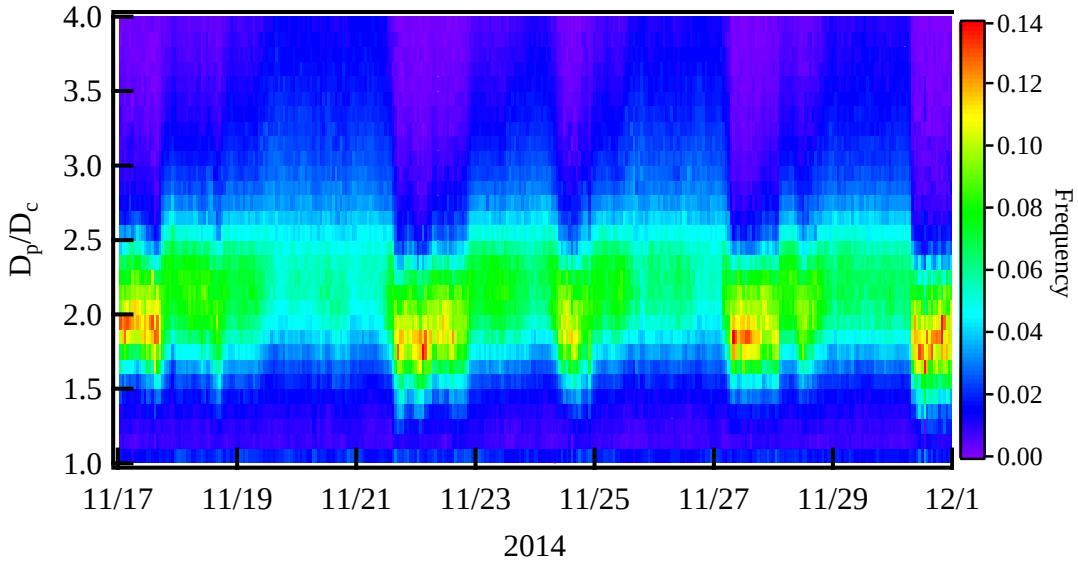

Figure S7. Frequency of the D_p/D_c ratio of BC-containing particles during the campaign period.

In this study, we used Mie mode to calculate optical properties of all BC-containing particles including bare BC and aged BC. Note that Mie theory is fundamentally ill-suited to calculation of optical properties for bare BC particles, which would lead to an underestimate of their light absorption. Based on the ratio between absorption predictions of Rayleigh-Debye-Gans (RDG) theory and Mie theory for size-resolved bare BC particles shown by Bond and Bergstrom (2006), we estimated that the absorption of bare BC observed in our site (most of rBC particles with size in the range of 90-200 nm, Fig. S4) using Mie theory with refractory index of 2.26-1.26i was underestimated by no more than 50%. Figure S7 shows that the bare BC particles (namely D_p/D_c smaller than 1.1) only accounted for ~3% of total BC particles during the campaign period. Therefore, the uncertainty of BC light absorption from the calculation of bare BC properties using Mie theory is no more than 2%.

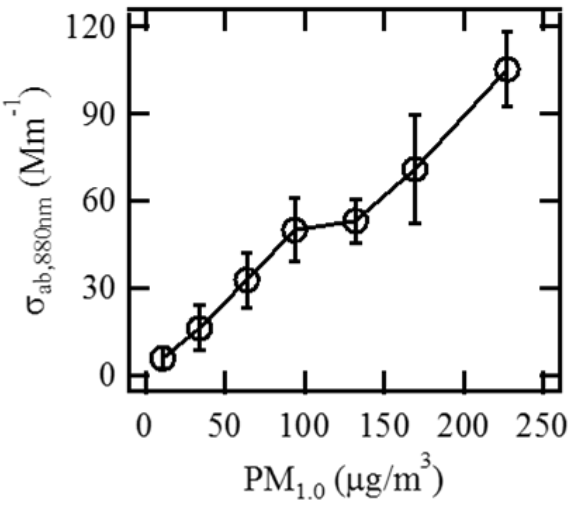

Figure S8. Changes of the light absorption coefficient at 880 nm ($\sigma_{ab,880nm}$) with PM_1 mass concentrations.

Figure S8 shows the changes of the light absorption coefficient at 880 nm ($\sigma_{ab,880nm}$) with PM_1 mass concentrations. The $\sigma_{ab,880nm}$ and rBC mass concentrations increased with increasing PM_1 mass concentrations. The increase of $\sigma_{ab,880nm}$ (~18 fold from ~10 μg m^{-3} of PM_1 to ~230 μg m^{-3} of PM_1) could be attributed to simultaneous increase in the rBC mass concentration and the amount of coating materials on the BC surface.

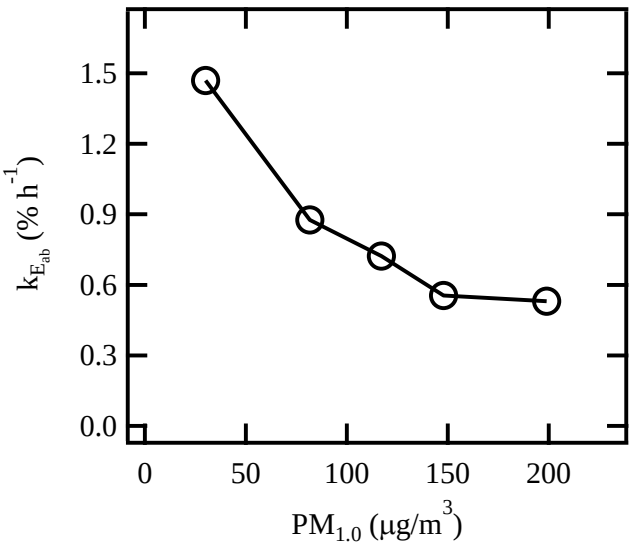

Figure S9. Changes of growth rate of E_{ab} (k_{Eab}) with PM1 mass concentration.

As shown in Figure S9, the changes of growth rate of E_{ab} (k_{Eab}) decreased with increasing PM_1 mass concentration. During the campaign period, the k_{Eab} of BC-containing particles was in the 0.5-1.5% h^{-1}. The decrease of k_{Eab} associated with air pollution indicated the enhancement of light absorption capability of BC-containing particles slowed with further air pollution, because BC aging process by condensational growth was less effective for more-aged BC particles with larger size under more pollution environment (Fig. S6).

1 Table S1. Previous studies on the BC and PM (PM_1 or $PM_{2.5}$) mass concentrations in China.

Site	Measurement Period	PM ($\mu g\ m^{-3}$)	BC ($\mu g\ m^{-3}$)	Reference
Beijing (urban site)	1 to 31 January 2013	$PM_{2.5}$: ~4.4-855 (mean: 162)	~0.2-25	Zheng et al., 2015
Xi'an, Shaanxi (urban site)	23 December 2012 to 18 January 2013	$PM_{2.5}$: ~10-600	~0.3-44.5 (mean: 8.8)	Wang et al., 2014
Nanjing, Jiangsu (urban site)	1 January to 31 December 2015	PM_1: ~10-250 (mean: 48)	~0.5-20 (mean: 2.9)	Zhao et al., 2017
Shanghai (urban site)	5 to 10 December 2013	$PM_{2.5}$: ~40-636 (mean: 221)	~0.6-12.1 (mean: 3.2)	Gong et al., 2016
Jiaxing, Zhejiang (suburban site)	29 June to 15 July 2010 11 to 23 December 2010	PM_1: Summer ~4.6-104 (mean: 32.9) Winter 5.8-160 (mean: 41.9)	Summer ~0.4-11.7 (mean: 3.0) Winter ~0.52-49.5 (mean: 7.1)	Huang et al., 2013
Guangzhou, Guangdong (urban site)	5 October to 5 November 2004	$PM_{2.5}$: ~63-152 (mean:103)	~3-20 (mean:103)	Andreae et al., 2008
Heshan, Guangdong (suburban site)	From 21 November to 1 December 2010	$PM_{2.5}$: 23.5-145.2 (mean: 74.6)	2.9-13.8 (mean: 8.2)	Zhang et al., 2014

Table 1 lists the BC and PM (PM_1 or $PM_{2.5}$) mass concentrations in China in previous study. In this study, the PM_1 and rBC concentrations were 10-230 μg m^{-3} and 0.3-12μg m^{-3} in Beijing during the campaign period (17 to 30 November 2014), which was consistent with previous studies in other polluted regions in China (Table 1). The consistency indicated that the enhancement of the light absorption capability of BC-containing particles associated with air pollution not only occurred in Beijing but also might be observed in other polluted regions in China.

References

Andreae, M. O., Schmid, O., Yang, H., Chand, D., Zhen Yu, J., Zeng, L.-M., and Zhang, Y.-H.: Optical properties and chemical composition of the atmospheric aerosol in urban Guangzhou, China, *Atmos. Environ.*, 42, 6335-6350, 2008.

Bond, T. C., and Bergstrom, R. W.: Light Absorption by Carbonaceous Particles: An Investigative Review, *Aerosol Sci. Technol.*, 40, 27-67, 2006.

Cappa, C. D., Onasch, T. B., Massoli, P., Worsnop, D. R., Bates, T. S., Cross, E. S., Davidovits, P., Hakala, J., Hayden, K. L., Jobson, B. T., Kolesar, K. R., Lack, D. A., Lerner, B. M., Li, S.-M., Mellon, D., Nuaaman, I., Olfert, J. S., Petäjä, T., Quinn, P. K., Song, C., Subramanian, R., Williams, E. J., and Zaveri, R. A.: Radiative Absorption Enhancements Due to the Mixing State of Atmospheric Black Carbon, *Science*, 337, 1078-1081, 2012.

Drinovec, L., Močnik, G., Zotter, P., Prévôt, A., Ruckstuhl, C., Coz, E., Rupakheti, M., Sciare, J., Müller, T., and Wiedensohler, A.: The" dual-spot" Aethalometer: an improved measurement of aerosol black carbon with real-time loading compensation, *Atmos. Meas. Tech.*, 8, 1965-1979, 2015.

Gong, X., Zhang, C., Chen, H., Nizkorodov, S. A., Chen, J., and Yang, X.: Size distribution and mixing state of black carbon particles during a heavy air pollution episode in Shanghai, Atmos. Chem. Phys., 16, 5399-5411, 2016.

Huang, X.-F., Xue, L., Tian, X.-D., Shao, W.-W., Sun, T.-L., Gong, Z.-H., Ju, W.-W., Jiang, B., Hu, M., and He, L.-Y.: Highly time-resolved carbonaceous aerosol characterization in Yangtze River Delta of China: Composition, mixing state and

secondary formation, *Atmos. Environ.*, 64, 200-207, 2013.

Segura, S., Estellés, V., Titos, G., Lyamani, H., Utrillas, M. P., Zotter, P., Prévôt, A. S. H., Močnik, G., Alados-Arboledas, L., and Martínez-Lozano, J. A.: Determination and analysis of in situ spectral aerosol optical properties by a multi-instrumental approach, *Atmos. Meas. Tech.*, 7, 2373–2387, 2014.

Taylor, J. W., Allan, J. D., Liu, D., Flynn, M., Weber, R., Zhang, X., Lefer, B. L., Grossberg, N., Flynn, J., and Coe, H.: Assessment of the sensitivity of core / shell parameters derived using the single-particle soot photometer to density and refractive index, *Atmos. Meas. Tech.*, 8, 1701-1718, 2015.

Wang, Q., Huang, R. J., Cao, J., Han, Y., Wang, G., Li, G., Wang, Y., Dai, W., Zhang, R., and Zhou, Y.: Mixing State of Black Carbon Aerosol in a Heavily Polluted Urban Area of China: Implications for Light Absorption Enhancement, *Aerosol Sci. Technol.*, 48, 689-697, 2014.

Weingartner, E., Saathoff, H., Schnaiter, M., Streit, N., Bitnar, B., and Baltensperger, U.: Absorption of light by soot particles: determination of the absorption coefficient by means of aethalometers, *J. Aerosol Sci.*, 34, 1445–1463, 2003.

Zhang, G., Bi, X., He, J., Chen, D., Chan, L. Y., Xie, G., Wang, X., Sheng, G., Fu, J., and Zhou, Z.: Variation of secondary coatings associated with elemental carbon by single particle analysis, *Atmos. Environ.*, 92, 162-170, 2014.

Zhao, Q., Shen, G., Li, L., Chen, F., Qiao, Y., Li, C., Liu, Q., and Han, J.: Ambient Particles (PM10, PM2.5 and PM1.0) and PM2.5 Chemical Components in Western Yangtze River Delta (YRD): An Overview of Data from 1-year Online Continuous Monitoring at Nanjing, *Aerosol Sci. Eng.*, 2017.

Zheng, G. J., Duan, F. K., Su, H., Ma, Y. L., Cheng, Y., Zheng, B., Zhang, Q., Huang, T., Kimoto, T., Chang, D., Pöschl, U., Cheng, Y. F., and He, K. B.: Exploring the severe winter haze in Beijing: the impact of synoptic weather, regional transport and heterogeneous reactions, *Atmos. Chem. Phys.*, 15, 2969-2983, 2015.